Biophysical and Molecular-Dynamics Studies of Phosphatidic Acid Binding by the Dvl-2 DEP Domain

Daniel G. S. Capelluto,[†*] Xiaolin Zhao,[†] Andrew Lucas,[†‡] Justin A. Lemkul,[§] Shuyan Xiao,[†] Xiangping Fu,[‡] Furong Sun,[†] David R. Bevan,[§] and Carla V. Finkielstein[‡]

[†]Protein Signaling Domains Laboratory, [‡]Integrated Cellular Responses Laboratory, Department of Biological Sciences, Virginia Bioinformatics Institute, and [§]Department of Biochemistry, Virginia Tech, Blacksburg, Virginia

ABSTRACT The Wnt-dependent, β-catenin-independent pathway modulates cell movement and behavior. A downstream regulator of this signaling pathway is Dishevelled (Dvl), which, among other multiple interactions, binds to the Frizzled receptor and the plasma membrane via phosphatidic acid (PA) in a mechanism proposed to be pH-dependent. While the Dvl DEP domain is central to the β-catenin-independent Wnt signaling function, the mechanism underlying its physical interaction with the membrane remains elusive. In this report, we elucidate the structural and functional basis of PA association to the Dvl2 DEP domain. Nuclear magnetic resonance, molecular-dynamics simulations, and mutagenesis data indicated that the domain interacted with the phospholipid through the basic helix 3 and a contiguous loop with moderate affinity. The association suggested that PA binding promoted local conformational changes in helix 2 and β-strand 4, both of which are compromised to maintain a stable hydrophobic core in the DEP domain. We also show that the Dvl2 DEP domain bound PA in a pH-dependent manner in a mechanism that resembles deprotonation of PA. Collectively, our results structurally define the PA-binding properties of the Dvl2 DEP domain, which can be exploited for the investigation of binding mechanisms of other DEP domain-interacting proteins.

INTRODUCTION

Proteins interact with membranes, and depending on the mode of their association, are usually classified as peripheral or integral. Peripheral proteins contact membranes through different surface moieties, whereas integral proteins insert into lipid bilayers. A well-characterized peripheral protein is Dishevelled (Dvl), which is the branch point of the canonical Wnt/β-catenin signaling pathway. It regulates cell-fate specification and proliferation, and participates in the noncanonical Wnt/planar cell polarity (PCP) pathway to control cell polarization, among other functions (1). Dysregulation of Wnt signaling is often associated with human birth defects, cancer, neurodegeneration, and osteoporosis (2,3). Whereas Wnt proteins trigger Dvl phosphorylation (4) and Dvl-dependent signalosome formation at the boundaries of the plasma membrane in the canonical Wnt signaling pathway (5), an asymmetric membrane association of Dvl is observed in the Wnt/PCP signaling branch (6). However, it is unknown whether Dvl employs the same mechanism of membrane targeting in both pathways. In the Wnt/β-catenin signaling pathway, the absence of Wnt facilitates the formation of a destruction complex that leads to cytosolic β-catenin degradation. Binding of a specific Wnt protein to both the Frizzled (Fz) receptor and LDL-related protein 5/6 coreceptor complex promotes Dvl recruitment to the plasma membrane in complex with axin, a scaffolding protein required for formation of the β-catenin destruction complex. Axin sequestration by Dvl results in dissociation of the β-catenin destruction complex, resulting in β-catenin accumulation and nuclear translocation, which facilitates Wnt-responsive gene transcription. The role of Dvl in noncanonical Wnt pathways is less clear. The PCP pathway relies on formation of the protein complexes that are asymmetrically distributed in the cell. During *Drosophila* wing cell polarization, Dvl accumulates distally in complex with other PCP proteins but is rarely found proximally (7).

Dvl proteins are multifunctional scaffold proteins with three highly related isoforms in mammals (Dvl1, 2, and 3) but with only one form found in *Drosophila* (8). The expression patterns of these isoforms overlap significantly during mouse development, suggesting that they have redundant functions, although unique functional regions have been identified in Dvl3 (9). Dvl proteins consist of several modules, including DIX (Dishevelled and axin), PDZ (postsynaptic density 95, disk large, and zonula occludens-1), and DEP (Dishevelled, Egl-10, and pleckstrin) domains. All three Dvl domains are critical in the canonical Wnt pathway (10). Both PDZ and DEP, but not DIX, are necessary for function of the PCP pathway (10). The DIX domain is involved in the formation of Dvl dynamic polymers, axin, actin, and vesicular association (11–13), whereas the PDZ domain binds to the Fz receptor, which is necessary to amplify Wnt signaling to downstream effectors (14). The DEP domain is a conserved module also found in Egl-10, pleckstrin, and within the regulator of the G protein signal family including Epac2, the R7 subfamily, and the yeast Sst2 proteins (15). The C-terminal DEP domain is involved in Dvl membrane targeting and Frizzled interactions (16).

Submitted October 30, 2013, and accepted for publication January 27, 2014.

*Correspondence: capellut@vt.edu

Xiaolin Zhao and Andrew Lucas contributed equally to this work.

Editor: Scott Feller.

0006-3495/14/03/1101/11 $2.00

http://dx.doi.org/10.1016/j.bpj.2014.01.032

The tertiary structure of several DEP domains displays a common α/β fold with some differences in the number of α/β elements (17–19). The presence of a cluster of basic residues on the DEP domain surface is suggested to be critical for Dvl membrane targeting (17). More recently, Simons et al. (20) initially characterized Dvl1 DEP domain association to the plasma membrane and proposed a mechanism in which basic residues, located in helix 3, would preferentially bind phosphatidic acid (PA). As a result, the DEP-PA association has been proposed to depend on intracellular pH, as demonstrated by the role of the Na^+/H^+ exchanger Nhe2 studies (20).

To obtain further insights into the membrane-binding properties of Dvl, we carried out structural, biochemical, mutagenesis, and molecular-dynamics simulation studies of the interaction of the Dvl2 DEP domain with PA. By obtaining the backbone resonance assignments of the Dvl2 DEP domain and monitoring the nuclear magnetic resonance (NMR) chemical shift changes of the protein induced by PA, we experimentally identified the amino acids directly and indirectly associated with lipid binding. Whereas helix 3 and a conserved loop region between β-strand elements 3 and 4 are compromised in PA ligation, conformational changes in the protein could occur in helix 2 and β-strand 4. Our results also indicate that PA recognition by Dvl2 DEP domain is pH-dependent and occurs with modest affinity, emphasizing that membrane targeting of Dvl should be facilitated by additional interactions of the domain with Fz at nonoverlapping sites.

MATERIALS AND METHODS

NMR spectroscopy

NMR samples contained 0.1–1 mM of uniformly ^{15}N and $^{15}N,^{13}C$ Dvl2 DEP domain, 90%H_2O/10% ^2H_2O, 20 mM d_4-sodium citrate (pH 5.5–7.5) buffer, 100 mM NaCl, 1 mM d_{10}-dithiothreitol, and 1 mM NaN_3. Lipid binding was monitored after chemical shift perturbations in the $^1H,^{15}N$ heteronuclear single quantum coherence (HSQC) spectra of 100-μM Dvl2 DEP domain after addition of 16-fold excess of dihexanoyl PA (DHPA; Avanti Lipids, Alabaster, AL), and was acquired at 25°C using an Avance III 600 MHz spectrometer (Bruker, Billerica, MA) equipped with triple-detection standard probes with z-axis pulse field gradients. The pH of the protein sample was confirmed and adjusted if needed before each run. Chemical shift perturbations were calculated according to the following formula (21):

$$\Delta\delta(^1H,^{15}N) = \left[(\Delta\delta^1H)^2 + (\Delta\delta^{15}N)^2/6\right]^{0.5}.$$

Triple-resonance experiments of $^{15}N,^{13}C$ Dvl2 DEP domain (1 mM) were performed at 25°C on INOVA 600 and 500 MHz spectrometers (Varian, Cary, NC) equipped with triple-resonance shielded probes with z-axis pulse field gradients. ^1H chemical shifts were referenced using sodium 4,4-dimethyl-4-silapentane-1-sulfonate (50 μM) as an internal reference. Sequential assignments of the backbone ^1H, ^{13}C, and ^{15}N resonances were made from $^1H,^{15}N$-HSQC, CBCA(CO)NNH, HNCACB, HNCO, and H(CCO)NH two-dimensional NMR spectroscopy experiments (τ_{mix} = 50 and 135 ms) (22–24). Spectra were processed with the software NMRPIPE (National Institutes of Health, Bethesda, MD) (25) and analyzed using the softwares PIPP (National Institutes of Health, Bethesda, MD) (26) and NMRDRAW (National Institutes of Health, Bethesda, MD). The resonance assignments of the Dvl2 DEP domain have been deposited in the Biological Magnetic Resonance Data Bank under accession No. 19584.

Molecular-dynamics simulations

The mouse Dvl2 DEP domain structure was generated by homology modeling based on its sequence identity (69.7%) to mouse Dvl1 DEP (PDB:1FSH; residues 404–502) using AL2TS (http://proteinmodel.org/AS2TS/AL2TS/al2ts.html) and validated using the SWISSMODEL workspace (http://swissmodel.expasy.org/). The stability of the Dvl2 DEP domain structure over time was judged by its root-mean-square deviation and root-mean-square fluctuation parameters (see Fig. S1 in the Supporting Material). All simulation preparation steps and analyses were conducted using the GROMACS software package, Vers. 3.3.3 (http://www.gromacs.org/) (27). All elements of the system were described by the GROMOS96 43A1 force field (28). Periodic boundary conditions were applied in all directions. The van der Waals interactions were truncated at 1.4 nm, with dispersion correction applied to energy and pressure terms to account for truncation. Nonbonded interactions were calculated using a twin-range scheme, updating the neighbor list between 0.9 and 1.4 nm every five simulation steps. The long-range electrostatics was calculated with the smooth particle-mesh Ewald method (29,30), using fourth-order spline interpolation and a Fourier grid spacing of 0.12 nm. The real-space contribution to particle-mesh Ewald was truncated at 0.9 nm. Simulations were carried out using a leapfrog integrator with an integration time step of 2 fs. All bonds within protein and lipid molecules were constrained using the LINCS algorithm (31) and water molecules were kept rigid using the SETTLE algorithm (32). All systems were energy-minimized using the steepest-descent method.

For each simulation, three independent trajectories were produced by generating different random velocities at the outset of equilibration, which was carried out in two phases. The initial phase employed a canonical (NVT) ensemble for 100 ps. Temperature was regulated using the Berendsen weak coupling method (33). Isothermal-isobaric (NPT) equilibration was then carried out for an additional 100 ps, using the Berendsen weak coupling method to regulate pressure at 1.0 bar. During equilibration, position restraints were placed on the heavy atoms of the DEP domain. Production simulations were carried out for 20 ns in the absence of any restraints, using the same ensemble as in the NPT stage. In the case of simulations in the presence of DHPA, the DEP domain was centered in a dodecahedral simulation box with four DHPA molecules randomly distributed around the protein in three different configurations. This setup suitably matches the molar ratio of protein/lipid used in the NMR experiments while avoiding any concentration-dependent artifacts that would arise from using a 1:16 protein/lipid.

The box was filled with simple point-charge water (34) and 100 mM NaCl. Parameters for DHPA were taken from the headgroups and first six carbons of the palmitoyl oleoyl PA (POPA) acyl chains (35), substituting a methyl group instead of a methylene for the sixth carbon in each acyl chain. Equilibration and simulation parameters are described above, with simulations conducted at 25°C, corresponding to experimental conditions. The configuration for the POPA membrane was taken from simulations conducted by Dickey and Faller (35), applying the same force-field parameters used in that work. The charge assigned to each lipid headgroup was –1. The system was then solvated with simple point-charge water (34), followed by the addition of 100 mM NaCl, giving a final system containing ~29,000 atoms. The system temperature was set at 37°C, above the phase-transition temperature of POPA (35). Pressure was regulated semiisotropically using the Berendsen method with a 2.0-ps coupling constant, allowing the membrane to deform independently in the x-y, and z dimensions. The electrostatic potential surfaces were calculated using the software DELPHI (http://compbio.clemson.edu/delphi.php) (36).

RESULTS

Backbone assignments of the Dvl2 DEP domain

To structurally characterize the Dvl2 DEP domain interaction with PA, we assigned the NMR backbone resonances of the protein. The backbone amide resonances in the $^{1}H,^{15}N$ HSQC spectra as well as the α- and β-carbons were sequentially assigned to all non-proline residues based on an analysis of the correlations observed in CBCA(CO)NH and HNCACB spectra. The backbone carbonyl resonance assignments were obtained from the HNCO and HN(CA)CO experiments, and the assignments for the α- and β-protons were obtained from the HBHA(CO)NH experiment. Ninety-five percent of $^{1}H_{N}$ and ^{15}N resonances of 95 backbone amides (excluding the three Pro residues) (Fig. 1) and ^{13}C resonances of 92 of the 99 backbone carbonyls of the Dvl2 DEP were assigned. NMR signals from four residues (Ile^{449}, Glu^{471}, Ser^{498}, and Glu^{499}) could not be assigned. In addition, 96% of Cα and 97% of Cβ resonances were assigned. The sequential connectivity of $^{13}C\alpha$ and $^{13}C\beta$ carbons of a representative region of the Dvl2 DEP domain is depicted in Fig. S2.

Structural analysis of Dvl2 DEP domain interaction with PA

Previous work, using a site-directed mutagenesis approach, demonstrates that the Dvl1 DEP domain binds acidic phospholipids with a preference for PA (20). However, the mutagenesis design is based on the exposed positively charged residues in the protein without any evidence of a direct role of these amino acids in lipid recognition. To precisely map the interaction surface between the Dvl2 DEP domain and PA, we titrated water-soluble DHPA into the ^{15}N-labeled Dvl2 DEP domain and monitored chemical shift perturbations in ^{1}H-^{15}N HSQC spectra. Several chemical shift changes and line-broadenings were observed at saturating concentrations of DHPA (Fig. 2, *A* and *B*).

Two distinct regions, located at the second helix (residues 461–469) and the fourth β-strand (residues 501–504) of the Dvl2 DEP were perturbed by DHPA (Fig. 2 *B*). Additional backbone perturbations were observed in the DEP N-terminal residues Ser^{418} and His^{420} as well as in resonances corresponding to His^{490}, and Lys^{494}, which are located between β-strand 3 and 4 near the C-terminus of the protein. Also, severe line-broadening of NMR signals were found in residues Asp^{422}, Leu^{445}, Met^{448}, Thr^{491}, Val^{492}, and Lys^{494}. By mapping the resonance perturbations on the structure of the Dvl2 DEP domain (Fig. 2 *C*), we concluded that two distinct regions on opposite sides of the protein may be involved in PA binding and/or they underwent a conformational change upon ligand association. The Dvl2 DEP domain bound to PA in a fast exchange regime on the NMR timescale, indicating that the lipid was weakly bound. DHPA-induced local conformational changes of the Dvl2 DEP domain was followed by monitoring the intrinsic fluorescence of two conserved Trp residues in the protein (Trp^{444} and Trp^{461}; see Fig. S3, *purple boxes*). Whereas Trp^{461} is located in helix 2, Trp^{444} is found between β-strands 1 and 2. Interestingly, chemical shift perturbation analysis indicated that the backbone amide resonance of Trp^{461} shifted in the presence of DHPA (Fig. 2 *A*). The observed Dvl2 DEP fluorescence emission trace between 310 and 410 nm was broad, likely due to the presence of Trp^{444} and Trp^{461}

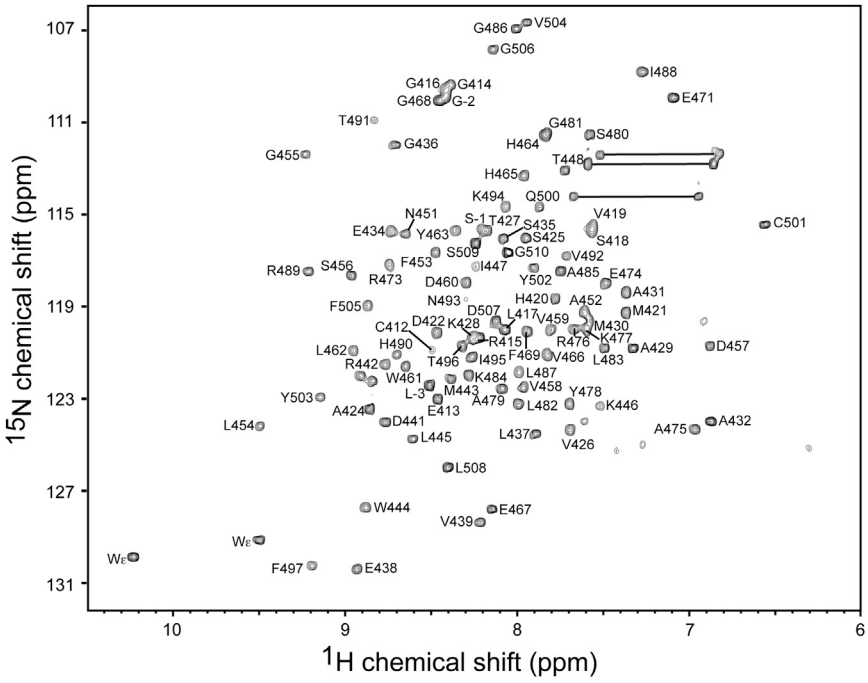

FIGURE 1 Backbone amide resonance assignments of the Dvl2 DEP domain. ^{15}N, ^{1}H HSQC spectrum of ^{15}N-labeled Dvl2 DEP domain. Selected peaks are labeled with the corresponding residue numbers. Residues from the vector are shown with negative numbers.

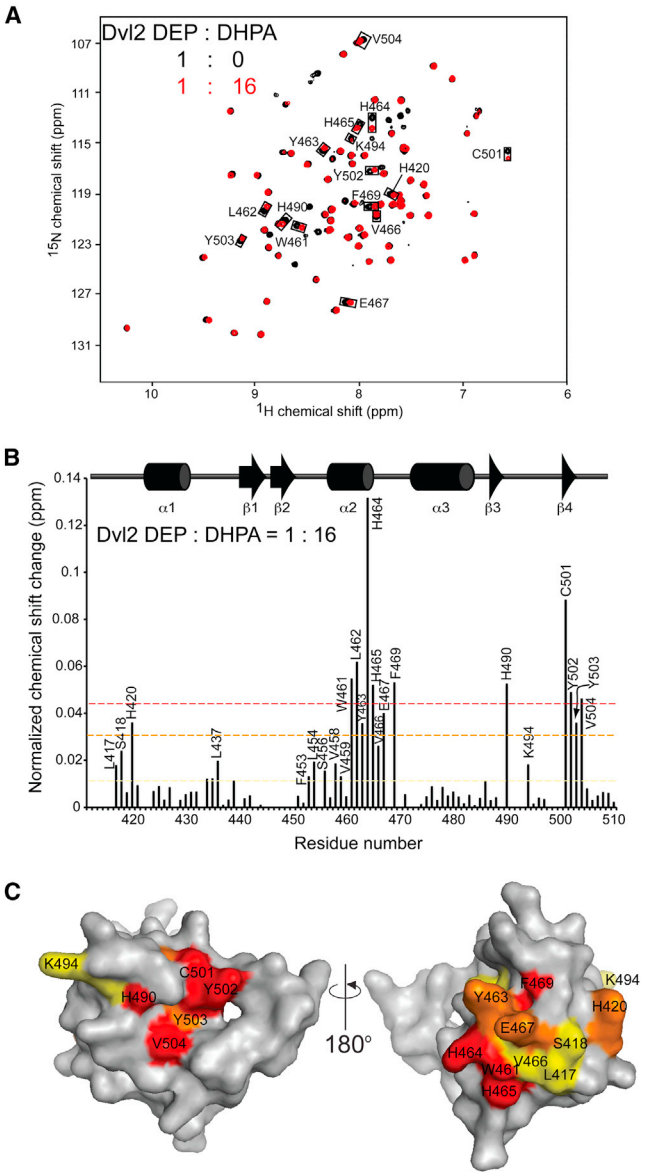

FIGURE 2 Contribution of Dvl2 DEP residues to PA binding. (*A*) ^{1}H,^{15}N HSQC spectra of ^{15}N-labeled DEP domain in the absence and presence of 16-fold DHPA are superimposed and color-coded (as shown in the key). (*Boxed* and *labeled*) Resonances of amino acids displaying chemical shift changes upon DHPA binding. (*B*) The histogram shows normalized chemical shift perturbations in the backbone amides of Dvl2 DEP domain induced by DHPA. (*Colored dashed lines*) Significant changes, based on the magnitude of their associated chemical shifts changes (*red*, $\Delta\delta_{average} + 2 \times$ standard deviation $\rightarrow$ *orange*, $\Delta\delta_{average} + 1.5 \times$ standard deviation $\rightarrow$ *yellow*, $\Delta\delta_{average}$). (*C*) Residues that exhibit significant chemical shift perturbations in panel *A* are labeled on the Dvl2 DEP surface and color-coded according to the scale defined in panel *B*. To see this figure in color, go online.

in distinct microenvironments (Fig. 3). Fluorescence emission of Dvl2 DEP domain was quenched by DHPA, suggesting solvent accessibility of the Trp residue/s of the protein upon DHPA binding, and saturated at 32-fold excess of the ligand (Fig. 3) with a K_D for DHPA of 4.30 $\pm$ 0.66 μM ($\chi_2 = 0.00009$).

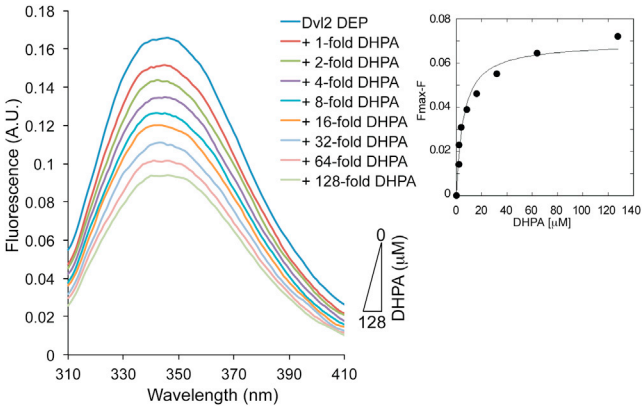

FIGURE 3 Dvl2 DEP domain PA-binding properties. Representative tryptophan fluorescence emission spectra of the Dvl2 DEP domain at the indicated DHPA molar ratios. (*Inset*) Plot of the reduction of the fluorescence emission of Dvl2 DEP domain against DHPA concentration. To see this figure in color, go online.

Far-UV circular dichroism (CD) analysis of the Dvl2 DEP indicates that the protein exhibited a characteristic spectrum of an α/β protein (see Fig. S4 *A*). Addition of DHPA did not induce major changes in the far-UV spectrum of the protein (see Fig. S4 *A*). Although the far-UV CD results show that no significant changes in secondary structure are present, evaluation of the near-UV CD spectra was carried out to confirm that the reduction of fluorescence intensity observed upon DHPA binding is indeed reflecting conformational changes in the Dvl2 DEP domain. The near-UV CD spectrum, which indicates the presence of tertiary structure in the protein, exhibited significant optical activity arising from the four Tyr and two Trp residues of the DEP domain in the 275–300 nm region and a positive signal at 260 nm, probably associated with the four Phe residues present in the DEP domain (see Fig. S4 *B*). A reduction of the amplitude of the CD signal is observed in the 255–265 and 290–300 nm regions when the protein is incubated with DHPA, indicating that the orientation of aromatic groups is perturbed in the DEP domain by the presence of the lipid. Overall, these observations, together with the comparison of ^{15}N,^{1}H HSQC, and intrinsic fluorescence of the free and PA-bound Dvl2 DEP domains, suggest that the protein undergoes a local conformational change upon DHPA binding rather than a major modification of the overall protein architecture.

Dvl2 DEP domain interaction with PA using molecular-dynamics simulations

In all simulations of the DEP domain in the presence of water-soluble DHPA, the lipid molecules are bound to the DEP domain within the first 10 ns of simulation time, after which their positions remained very stable. The final configurations of each of the three simulations are shown in Fig. 4 and details of such interactions are shown in Fig. S5,

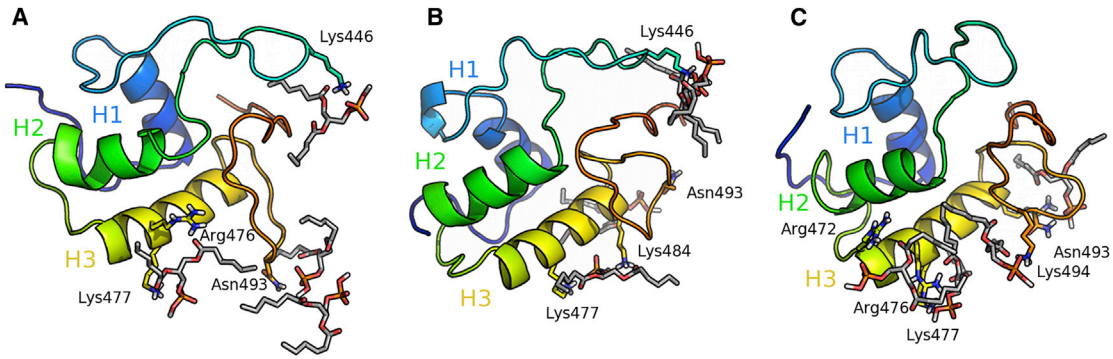

FIGURE 4 Interactions between Dvl2 DEP domain and DHPA for (*A*) simulation 1, (*B*) simulation 2, and (*C*) simulation 3. Residues that are responsible for binding DHPA lipids (*labeled*, displayed as *sticks*, and colored by element: C, *gray*; O, *red*; P, *gold*; H, *white*). The DEP domain is shown as a cartoon structure (and colored as a rainbow gradient from *blue*, N-terminus to *red*, C-terminus). (*Blue*, *green*, and *yellow*) Helices H1, H2, and H3 in the DEP domain, respectively. To see this figure in color, go online.

Fig. S6, Fig. S7, Table S1, and Table S2 in the Supporting Material. In two of the simulations, DHPA molecules bound to Asn^{493} via hydrogen bonds, an interaction that was further stabilized in one simulation by interactions with Lys^{494}; these residues are located in a flexible loop region that also was perturbed from NMR analysis (Fig. 2). DHPA was also coordinated by Lys^{446} in two simulations. In all three simulations, several DHPA molecules bound to the basic helix region of the DEP domain, specifically residues Arg^{472}, Arg^{476}, and Lys^{477}. Lys^{484}, a residue just beyond the C-terminus of the basic helix, also coordinated one DHPA molecule in one simulation. The results of the three independent simulations suggest that DHPA molecules primarily bind to arginine and lysine residues in the basic helix (residues 472–479) and in the flexible loop region that extends from the C-terminus of this helix.

Binding events between the DEP domain and the POPA membrane occurred in all three simulations within 1 ns of simulation time (Fig. 5; see details of such interactions in Fig. S8, Table S1, and Table S3) and involved many of the same residues that were observed in the DEP-DHPA simulations (Fig. 4). In all simulations, initial contacts made between the DEP domain and the POPA membrane involved Lys^{494}, which served to draw the protein downward to the membrane surface. Asn^{493} was also involved in the initial binding event via hydrogen bonding with the headgroups of the POPA lipids, but interactions involving Asn^{493} were only transient over time after the initial interactions. Binding of the DEP domain to POPA was further augmented by interactions involving Arg^{473} and Lys^{477}, residues in the basic helix 3 region of the domain. Transient interactions involving Arg^{472} and Arg^{476} were also observed in at least one of the three simulations. Interactions between POPA and DEP residues Arg^{473} and Lys^{477} were very strong, with each residue maintaining an average minimum distance of 0.2 nm or less with any POPA lipid over the course of the simulations. This distance was a result of very strong electrostatic and hydrogen-bonding interactions.

The DEP domain formed 17 $\pm$ 2 hydrogen bonds with POPA lipids, with 9 $\pm$ 2 of these involving residues in the basic helix region. Given that such a short sequence accounts for the majority of the hydrogen bonds between the DEP domain and POPA, these results indicate that the positively charged residues in the basic helix drive the association of the DEP domain with negatively charged POPA lipids. Once bound to the POPA surface, the DEP domain was able to diffuse in the *x*-*y* plane at an average rate of $3 \pm 3 \times 10^{-7}$ cm^2 s^{-1}, slightly faster than the lipids themselves, which diffused at an average rate of $2 \pm 2 \times 10^{-7}$ cm^2 s^{-1}. These findings indicate that the DEP domain remained tightly bound to the POPA membrane by virtue of electrostatic and hydrogen-bonding interactions, but these interactions could be exchanged between lipid molecules, allowing the DEP domain to move across the lipid surface.

Identification of critical residues in Dvl2 DEP engaged in PA binding

To distinguish between key Dvl2 DEP domain PA-interacting residues and conformational changes in the protein induced by the phospholipid, we carried out mutagenesis on residues that exhibited DHPA-mediated NMR chemical shift perturbations as well as on those residues that showed interactions with the lipid from molecular-dynamics simulations. We used two different lipid-binding assays. Mutations in residues His^{464}, His^{465}, and Phe^{469} did not significantly affect binding (Fig. 6 *A*), suggesting that local conformational changes, rather than direct interaction with the lipid, occur in and around the second helix of the protein. Mutations on the DEP domain residues His^{490} and Lys^{494}, which induced NMR chemical shift perturbations (Fig. 2) and interacted with DHPA in our simulation studies (Fig. 4), severely reduced PA binding (Fig. 6 *A*). We were unable to evaluate additional putative PA-interacting Dvl2 DEP domain residues, as suggested from NMR titration experiments, because alanine mutation of His^{420} and Lys^{462} and

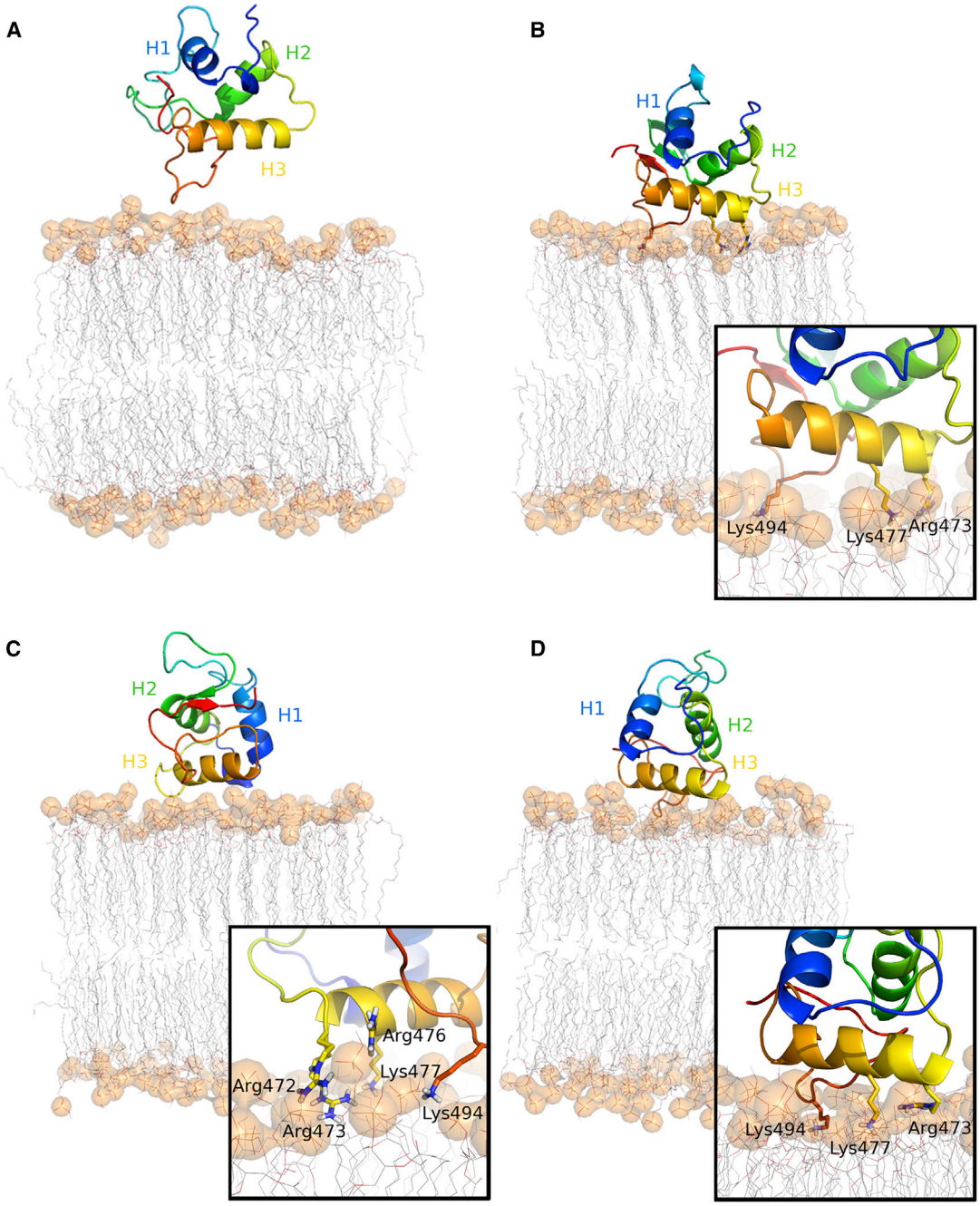

FIGURE 5 Snapshots of DEP-POPA interactions. (*A*) The starting configuration for the simulations. (*B–D*) The final snapshot from simulations 1–3. (*Insets*) Residues responsible for binding (*sticks*, *labeled*). The DEP domain is shown as a cartoon structure (and colored as a rainbow gradient from *blue*, N-terminus to *red*, C-terminus). (*Blue*, *green*, and *yellow*) Helices H1, H2, and H3 in the DEP domain, respectively. POPA lipids are drawn as lines and color by element (*gray*, C; *red*, O; *gold*, P; *white*, H). (*Translucent gold spheres*) Positions of phosphorus atoms. To see this figure in color, go online.

serine mutation of Cys^{501} produced misfolded or degraded products, as determined by CD spectroscopy and sodium dodecyl sulfate-polyacrylamide gel electrophoresis analyses (data not shown).

Studies on the Dvl1 DEP domain have shown that glutamic acid mutations of residues Lys^{408}, Lys^{458}, Lys^{465}, Lys^{472}, and Lys^{482}, which are equivalent to Dvl2 His^{420}, Pro^{470}, Lys^{477}, Lys^{484}, and Lys^{494}, respectively, abolish PA binding (20). Only resonances from the backbone amide groups of His^{420} and Lys^{494} (prolines are not visualized in HSQC spectra) were significantly perturbed by DHPA in Dvl2 DEP (Fig. 2). We also observed very minor perturbations of resonances mapping in helix 3, but they were not significant when compared with perturbations observed in helix 2 and β-strand 4 (Fig. 2 *B*). An alanine mutation of Lys^{477} (helix 3) reduced PA binding (Fig. 6), which was

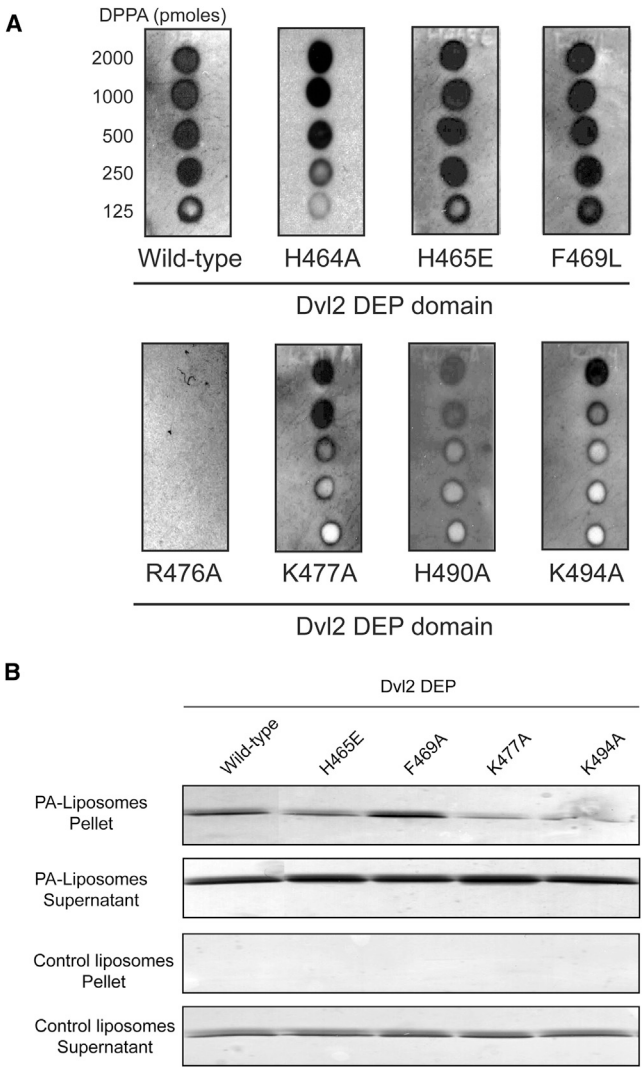

FIGURE 6 Identification of PA-binding residues of the Dvl2 DEP domain. (*A*) Lipid-protein overlay assay of GST-Dvl2 DEP and mutants as well as GST, as a negative control, were evaluated for dipalmitoyl PA (DPPA) binding. (*B*) Liposome binding assay for the Dvl2 DEP domain and mutants in the absence and presence of dioleoyl PA (DOPA). The figure shows representative experiments that were repeated three times with similar results.

consistent with our simulation studies (Fig. 4), indicating that the side chain, but not the backbone of the amino acid, may play an important role in the association. Moreover, alanine mutagenesis on Arg^{476} (which is also located in helix 3) abrogated lipid binding, supporting our simulation studies. Far-UV CD spectra of the most critical PA-binding mutants, such as K477A, and K494A, exhibited similar traces compared with the wild-type protein, indicating that mutations did not significantly perturb the global fold of the protein in these regions (see Fig. S9). As summarized in Table S4, our results identified the role of the third helix and a loop of the Dvl2 DEP domain, located between the third and fourth β-strand elements, in PA recognition.

Dvl2 DEP domain binding to PA is pH-dependent

Recent work by Simons et al. (20) proposes that Dvl recruitment to the membrane depends on pH-sensing by PA to regulate cell polarity in *Drosophila*. To biochemically determine the effect of the physiological pH range on the Dvl2 DEP domain binding of PA, we evaluated the association at pH values from 6.5 to 8.0. We found that the Dvl2 DEP dramatically decreased binding to PA at pH values below 8.0 (Fig. 7 *A*), whereas the Vam7p PX domain binding to PtdIns(3)P (phosphatidylinositol 3-phosphate) was not affected, consistent with previous observations (37). To quantify the pH effect using a membrane mimic that closely resembles a lipid bilayer, a liposome-binding assay was performed in a range of physiologically relevant pH values. The DEP domain was incubated with large unilamellar vesicles, without and with DOPA, at pH values of 6.25, 6.5, 6.8, 7.1, and 7.5 and unbound (supernatant) and liposome-bound Dvl2 DEP domain (pellet) fractions were obtained by centrifugation.

By increasing the pH from 6.25 to 7.5, the Dvl2 DEP domain increased its interaction with DOPA-containing liposomes by >50% (Fig. 7 *B*). This is in agreement with the observed defective *Drosophila* Dvl recruitment to the plasma membrane when the intracellular pH was dropped to pH 7.1 (20). A near-UV CD spectrum of Dvl2 DEP domain exhibited differences in their traces at pH values of 6.25 and 7.5 (see Fig. S10), suggesting that there are pH-dependent conformational changes around aromatic groups of the Dvl2 DEP domain. To better visualize this effect, we analyzed pH-dependent changes in the protein by collecting HSQC spectra at pH values of 5.5 and 7.5. Interestingly, and in agreement with the electrostatic/hydrogen-bond switch model (38), we observed that increasing the pH from 5.5 to 7.5 induced chemical shift perturbations in the Dvl2 DEP domain spectrum (Fig. 7 *C*) which, in most cases, mirrored the perturbations observed by the addition of DHPA (Fig. 2 *A*).

DISCUSSION

In this report, we precisely characterize the phospholipid binding properties of the Dvl2 DEP domain. A significant impact of the biophysical approach reported here is that it provides direct evidence for the DEP domain residues engaged in PA binding and it does so in a pH-dependent manner. As depicted in Fig. 8, the positive electrostatic potential of the Dvl2 DEP domain is distributed all over its surface at pH 5.5, whereas the positive charge is clearly localized on the PA-interacting regions, the helix 3 and a downstream loop, surrounded by negative charges at pH 7.5. This observation suggests that the DEP domain becomes more specific for its lipid ligand and that lipid binding is favored by electrostatic interactions with both helix 3 and its contiguous loop at higher pH values. The

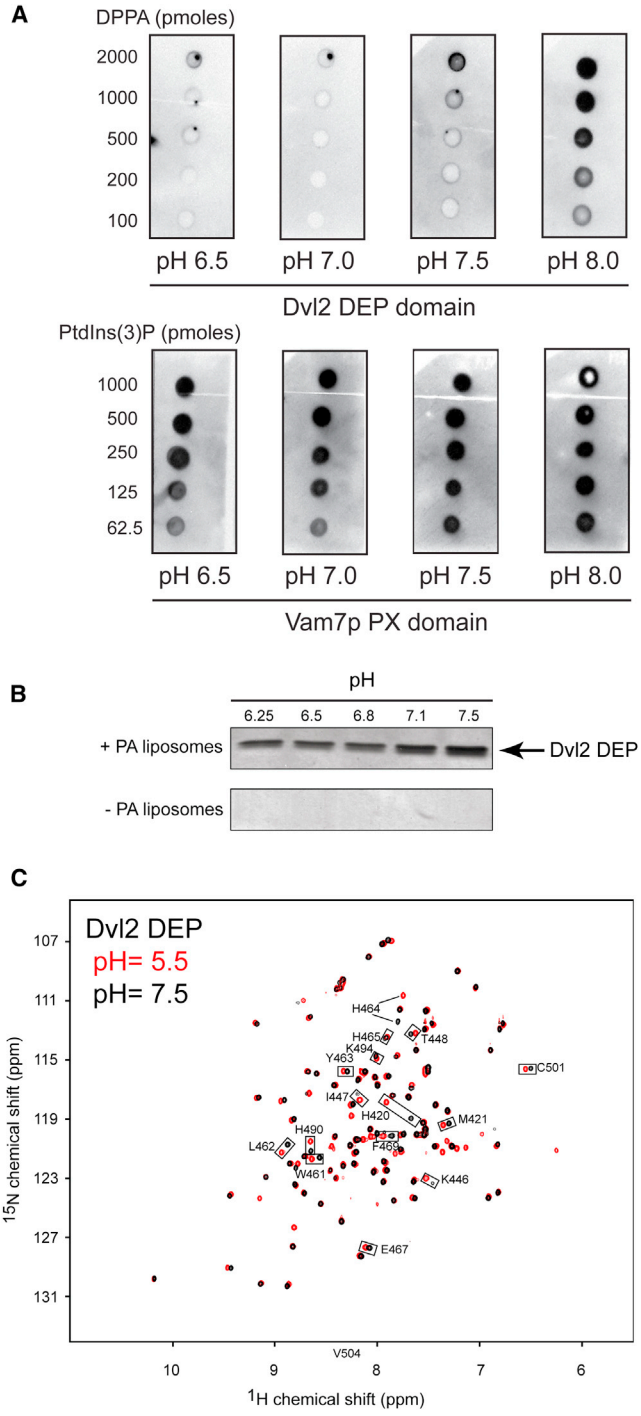

FIGURE 7 Binding of the Dvl2 DEP domain is pH-dependent. (*A*) Lipid-protein overlay assay of DPPA binding of Dvl2 DEP domain (*top*) and PtdIns(3)P binding of Vam7p PX domain (*bottom*) at the indicated pH values. (*B*) Representative gels of liposome pellets showing binding of Dvl2 DEP to DOPA-containing liposomes (*top*) and DOPA-free liposomes (*bottom*) at the indicated pH values. (*C*) ^{15}N-HSQC spectra of the Dvl2 DEP domain at pH 5.5 (*red*) and 7.5 (*black*). To see this figure in color, go online.

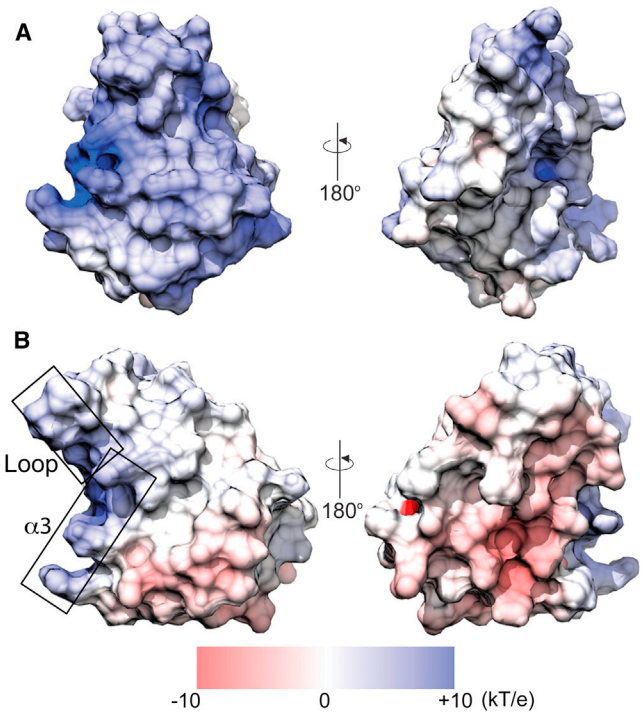

FIGURE 8 (*A* and *B*) Electrostatic potential surfaces for the DEP domain at pH 5.5 (*top*) and 7.5 (*bottom*). The corresponding electrostatic potential surfaces are colored as gradients (*red*, negative; *blue*, positive). (*Boxed*) Positive charge generated on the PA-interacting regions of the DEP domain at pH 7.5. To see this figure in color, go online.

three-dimensional structure of Dvl1 DEP domain has been solved by NMR spectroscopy (17). The structure reveals the presence of a three-helix bundle, a β-hairpin arm, and two short β-strand elements at the C-terminus of the domain. An almost identical structure has been determined for the Dvl2 DEP domain as a chimera in complex with the μ2 subunit of the AP-2 clathrin adaptor (39).

The major feature of the DEP domain structure is the presence of a hydrophobic core formed by the three α-helices, which maintain a stable tertiary structure. Based on the structure, a patch of basic residues in helix 3 of the Dvl1 DEP domain surface has been suggested to interact with acidic phospholipids on the plasma membrane (20). Basic residues also drive Epac1 DEP domains and Sst2 DEP interactions with phosphatidylserine, phosphatidylinositol 4,5-bisphosphate, and phosphatidylinositol 3,4,5-trisphosphate (40,41). In addition to the loop residues His^{490} and Lys^{494}, we observed NMR chemical shift perturbations of the Dvl2 DEP domain in backbone residues located at the helix 2 and β-strand 4 elements. Due to strong hydrophobic contacts of helix 2 with the functional helix 3, as well as the capping function of β-strand 4 on the hydrophobic core of the DEP domain (17), we therefore propose that lipid contact to the side chains of residues of helix 3 triggers both local pH and conformational changes in helix 2 and β-strand 4, which are

committed to maintaining the rigid hydrophobic core of the protein.

The DEP domain is required for Dvl recruitment to the plasma membrane during PCP- and β-catenin-mediated signaling (16,20). In addition, the Dvl DEP domain and a C-terminal region of the protein are responsible for the interaction with the Fz receptor to activate β-catenin-mediated signaling (16). Three motifs of Fz, two located in the third intracellular loop and one at the C-terminus of the protein, are required for binding to the Dvl central and C-terminal regions and trigger Wnt-induced β-catenin stabilization (14,16). Specifically, the Dvl1 PDZ (14) and DEP (16) domains preferentially bind to the Fz C-terminal region that contains the KTxxxW motif with K_D values of 10 and 22–30 μM, respectively, and that the Dvl1 residues Lys^{438}, Asp^{449}, and Asp^{452} (equivalent to Dvl2 Lys^{446}, Asp^{457}, and Asp^{460}, respectively) are required for this association (16). Interestingly, NMR resonances of these key Fz-interacting residues in Dvl2 are not perturbed by DHPA (Fig. 2), which makes them available for simultaneous binding with Fz and phospholipids (16). Likewise, structural analysis of the Dvl2 DEP-μ2 subunit of the AP-2 clathrin adaptor reveals that PA-independent DEP domain residues Asp^{441}, Lys^{446}, Asn^{451}, and Arg^{489} are compromised in μ2 subunit binding (39).

PA is a relatively abundant phospholipid (~1% of total cellular lipid (42)) that exhibits a cone-shaped structure, a conformation that prevents tight packing of the small headgroup of the phospholipid with the headgroups of other lipids found at the plasma membrane (43,44). PA-binding proteins lack the presence of a conserved PA-binding site, but instead interact with the phospholipid through nonspecific electrostatic interactions between patches of positively charged amino acids and the negatively charged headgroup of PA, whereas hydrophobic amino acids may contribute to membrane insertion (45). Indeed, basic residues such as lysine and arginine are hydrogen-bond donors because of the presence of primary amines in their side chains. Consequently, Kooijman et al. (38) proposed a mechanism by which PA is recognized by PA-binding proteins known as the electrostatic/hydrogen-bond switch mechanism. In this model, proteins initially recognize the single protonated form of PA, and upon recognition, the basic amino acids of the protein can form a hydrogen bond with the PA phosphomonoester headgroup, a reaction that triggers dissociation of a proton from PA leaving the phospholipid with a 2^- charge. A more negative form of PA facilitates electrostatic interactions with the protein, thus, making the protein-lipid complex more stable.

Our results demonstrate that the Dvl2 DEP domain third helix and a loop downstream of helix 3 are involved in PA binding. These regions are basic in nature, supporting the idea that the interaction of the protein with the lipid is mainly electrostatic. Biophysical data showed that two basic residues located in the loop, His^{490} and Lys^{494}, are relevant for the interaction. We were unable to observe perturbations in the HN backbone of the residues comprising helix 3, but both mutagenesis and molecular-dynamics simulations studies demonstrated the role of this region in PA binding, emphasizing the role of the side chains of the lipid-interacting residues. Binding locations of DHPA to the DEP domain were similar among all the simulations, and involved many of the same residues seen in the DEP-POPA simulations. The residues principally responsible for binding DHPA were polar (Lys^{446}, Arg^{472}, Arg^{476}, Lys^{477}, Lys^{484}, and Asn^{493}). This surface is capable of binding to not only the planar surface of the POPA membrane, but also soluble DHPA clustered over the positively charged protein surface.

In each of the three simulations of the Dvl2 DEP domain in the presence of POPA-containing lipid bilayers, initial contacts between the protein and the lipids were made through residues in the loop region comprising residues 491–497, most frequently Lys^{494}. The binding event was further stabilized through the involvement of lysine and arginine residues in the basic helix 3 extending from residues 472–479 of the protein. We could not visualize significant NMR perturbations by the addition of DHPA in backbone amide groups of helix 3 (Fig. 2). We suggest that changes may occur on their side chains, which cannot be observed in the frequency range tested in our NMR experiments. We demonstrated that single mutations of basic residues drastically reduced PA binding. This observation is in agreement with PA binding of mTOR and Epac1, in which their residues Arg^{2109} and Arg^{82}, respectively, are strictly required for lipid recognition (40,46,47). Interestingly, the mTOR Arg^{2109} side chain, but not its backbone amide, is perturbed by DHPA (47), a behavior that is likely observed for Lys^{477} in the Dvl2 DEP domain.

We biochemically demonstrated that PA binding of the Dvl2 DEP domain is pH-dependent, consistent with the proposed mechanism of Dvl membrane binding (20), and generally accepted for other PA recognition modules (45). Thus, differentially protonated states of the lipid will determine the interaction with surface-basic residues of the protein through electrostatic interactions. Membrane binding of a protein to PA, through its basic residues, introduces additional positive charges at the membrane. This association will decrease the proton content due to charge repulsion and, thus, promotes an increment of the local pH at the membrane. The second pK_a value for PA is between 6.9 and 7.9 (48), and, consequently at pH values higher than its second pK_a value, the majority of the lipid will be deprotonated and more prone to protein binding. Experimentally, we observed this phenomenon; increasing the pH value in the Dvl2 DEP domain NMR sample led to specific chemical shift changes that were also observed after the addition of DHPA.

In addition to PA, Wnt signaling-related proteins including Prickle, Rac1, and the muscle kinase receptor

have been shown to interact with the Dvl DEP domain by pull-down or immunoprecipitation assays (6,49,50). However, there is a lack of information about the mechanism of recognition of the complexes, their kinetic properties, and whether PA plays a role in these associations. Thus, the availability of the resonance assignments of the Dvl2 DEP domain and details of PA binding will provide the tools to monitor these associations at atomic resolution, map their binding sites, and understand how Dvl controls the equilibrium and divergence of multiple Wnt-dependent signaling pathways by its DEP domain.

CONCLUSIONS

We report details of the structural and functional basis of PA recognition by the Dvl2 DEP domain. The work shown here reveals distinctive features that have escaped previous attention, including that, in addition to helix 3, a loop between the β3 and β4 elements plays a role in PA recognition. Local conformational changes accompany binding and likely involve helix 2 and β-strand 4, both of which are tightly associated with the hydrophobic core of the DEP domain, which is important to maintain tertiary structure stability (17). More significantly, we demonstrated that mutations on single conserved basic residues in the DEP domain affect lipid binding, a property that has been found in other PA binding proteins (40,46,47). Given the modest affinity of the DEP domain to PA, additional molecular interactions should be present (e.g., Fz binding, ligation to other acidic phospholipids) for the formation of a stable Dvl membrane-binding complex. Furthermore, our identification of pH-dependent binding of the Dvl2 DEP domain not only supports the electrostatic/hydrogen-bond switch model (38), but also confirms recent findings that indicate that the association should be tightly modulated by changes in the intracellular pH, by the action of proton pumps (20) and, perhaps, by fluctuations in PA levels at the plasma membrane.

SUPPORTING MATERIAL

Four tables, 10 figures and references (51–53) are available at http://www.biophysj.org/biophysj/supplemental/S0006-3495(14)00133-7.

We thank Dr. Janet Webster for assistance during preparation of the manuscript and Dr. Michael Overduin for his initial support of this work. Additional thanks go to Advanced Research Computing at Virginia Tech for computing time. We are also grateful to Dr. Hugo Azurmendi, Abigail Ellis, Karla Sanchez, and My-Thanh Vo, for their contribution in the initial phase of this work.

This work was supported by the National Institutes of Health (grant No. R03HD065999 to D.G.S.C.).

REFERENCES

1. Dillman, A. R., P. J. Minor, and P. W. Sternberg. 2013. Origin and evolution of Dishevelled. *G3.* 3:251–262.
2. Clevers, H. 2006. Wnt/β-catenin signaling in development and disease. *Cell.* 127:469–480.
3. MacDonald, B. T., K. Tamai, and X. He. 2009. Wnt/beta-catenin signaling: components, mechanisms, and diseases. *Dev. Cell.* 17:9–26.
4. Lee, J. S., A. Ishimoto, and S. Yanagawa. 1999. Characterization of mouse Dishevelled (Dvl) proteins in Wnt/Wingless signaling pathway. *J. Biol. Chem.* 274:21464–21470.
5. Bilic, J., Y. L. Huang, …, C. Niehrs. 2007. Wnt induces LRP6 signalosomes and promotes Dishevelled-dependent LRP6 phosphorylation. *Science.* 316:1619–1622.
6. Tree, D. R., J. M. Shulman, …, J. D. Axelrod. 2002. Prickle mediates feedback amplification to generate asymmetric planar cell polarity signaling. *Cell.* 109:371–381.
7. Simons, M., and M. Mlodzik. 2008. Planar cell polarity signaling: from fly development to human disease. *Annu. Rev. Genet.* 42:517–540.
8. Semënov, M. V., and M. Snyder. 1997. Human Dishevelled genes constitute a DHR-containing multigene family. *Genomics.* 42:302–310.
9. Wang, H. Y., and C. C. Malbon. 2012. Dishevelled C-terminus: prolyl and histidinyl motifs. *Acta Physiol. (Oxf.).* 204:65–73.
10. Wallingford, J. B., and R. Habas. 2005. The developmental biology of Dishevelled: an enigmatic protein governing cell fate and cell polarity. *Development.* 132:4421–4436.
11. Kishida, S., H. Yamamoto, …, A. Kikuchi. 1999. DIX domains of Dvl and axin are necessary for protein interactions and their ability to regulate β-catenin stability. *Mol. Cell. Biol.* 19:4414–4422.
12. Schwarz-Romond, T., M. Fiedler, …, M. Bienz. 2007. The DIX domain of Dishevelled confers Wnt signaling by dynamic polymerization. *Nat. Struct. Mol. Biol.* 14:484–492.
13. Capelluto, D. G., T. G. Kutateladze, …, M. Overduin. 2002. The DIX domain targets Dishevelled to actin stress fibers and vesicular membranes. *Nature.* 419:726–729.
14. Wong, H. C., A. Bourdelas, …, J. Zheng. 2003. Direct binding of the PDZ domain of Dishevelled to a conserved internal sequence in the C-terminal region of Frizzled. *Mol. Cell.* 12:1251–1260.
15. Chen, S., and H. E. Hamm. 2006. DEP domains: more than just membrane anchors. *Dev. Cell.* 11:436–438.
16. Tauriello, D. V., I. Jordens, …, M. M. Maurice. 2012. Wnt/β-catenin signaling requires interaction of the Dishevelled DEP domain and C terminus with a discontinuous motif in Frizzled. *Proc. Natl. Acad. Sci. USA.* 109:E812–E820.
17. Wong, H. C., J. Mao, …, J. Zheng. 2000. Structural basis of the recognition of the Dishevelled DEP domain in the Wnt signaling pathway. *Nat. Struct. Biol.* 7:1178–1184.
18. Rehmann, H., B. Prakash, …, A. Wittinghofer. 2003. Structure and regulation of the cAMP-binding domains of Epac2. *Nat. Struct. Biol.* 10:26–32.
19. Civera, C., B. Simon, …, M. J. Macias. 2005. Structure and dynamics of the human pleckstrin DEP domain: distinct molecular features of a novel DEP domain subfamily. *Proteins.* 58:354–366.
20. Simons, M., W. J. Gault, …, M. Mlodzik. 2009. Electrochemical cues regulate assembly of the Frizzled/Dishevelled complex at the plasma membrane during planar epithelial polarization. *Nat. Cell Biol.* 11:286–294.
21. Gautier, A., H. R. Mott, …, D. Nietlispach. 2010. Structure determination of the seven-helix transmembrane receptor sensory rhodopsin II by solution NMR spectroscopy. *Nat. Struct. Mol. Biol.* 17:768–774.
22. Muhandiram, D. R., and L. E. Kay. 1994. Gradient-enhanced triple-resonance three-dimensional NMR experiments with improved sensitivity. *J. Magn. Reson.* 103:203–216.
23. Grzesiek, S., J. Anglister, and A. Bax. 1993. Correlation of backbone amide and aliphatic side-chain resonances in C-13/N-15-enriched proteins by isotropic mixing of C-13 magnetization. *J. Magn. Reson.* 101:114–119.

24. Kay, L. E., G. Y. Xu, …, J. D. Forman-Kay. 1993. A gradient-enhanced HCCH TOCSY experiment for recording side-chain H-1 and C-13 correlations in H_2O samples of proteins. *J. Magn. Reson.* 101:333–337.

25. Delaglio, F., S. Grzesiek, …, A. Bax. 1995. NMRPIPE: a multidimensional spectral processing system based on UNIX pipes. *J. Biomol. NMR.* 6:277–293.

26. Garrett, D. S., R. Powers, …, G. M. Clore. 1991. A common-sense approach to peak picking in two-dimensional, three-dimensional, and four-dimensional spectra using automatic computer-analysis of contour diagrams. *J. Magn. Reson.* 95:214–220.

27. van der Spoel, D., E. Lindahl, …, H. J. C. Berendsen. 2005. GROMACS: fast, flexible, and free. *J. Comput. Chem.* 26:1701–1718.

28. Scott, W. R. P., P. H. Hünenberger, …, W. F. van Gunsteren. 1999. The GROMOS biomolecular simulation program package. *J. Phys. Chem. A.* 103:3596–3607.

29. Darden, T., D. York, and L. Pedersen. 1993. Particle mesh Ewald: an $N\cdot\log(N)$ method for Ewald sums in large systems. *J. Chem. Phys.* 98:10089–10092.

30. Essmann, U., L. Perera, …, L. G. Pedersen. 1995. A smooth particle mesh Ewald method. *J. Chem. Phys.* 103:8577–8593.

31. Hess, B., H. Bekker, …, J. G. E. M. Fraaije. 1997. LINCS: a linear constraint solver for molecular simulations. *J. Comput. Chem.* 18:1463–1472.

32. Miyamoto, S., and P. A. Kollman. 1992. SETTLE: an analytical version of the SHAKE and RATTLE algorithms for rigid water models. *J. Comput. Chem.* 13:952–962.

33. Berendsen, H. J. C., J. P. M. Postma, …, J. R. Haak. 1984. Molecular dynamics with coupling to an external bath. *J. Chem. Phys.* 81:3684–3690.

34. Berendsen, H. J. C., J. P. M. Postma, …, J. Hermans. 1981. Interaction models for water in relation to protein hydration. *In* Intermolecular Forces. B. Pullman, editor. Reidel, Dordrecht, The Netherlands, p. 331.

35. Dickey, A., and R. Faller. 2008. Examining the contributions of lipid shape and headgroup charge on bilayer behavior. *Biophys. J.* 95:2636–2646.

36. Li, L., C. Li, …, E. Alexov. 2012. DelPhi: a comprehensive suite for DelPhi software and associated resources. *BMC Biophys.* 5:9.

37. Lee, S. A., J. Kovacs, …, T. G. Kutateladze. 2006. Molecular mechanism of membrane docking by the Vam7p PX domain. *J. Biol. Chem.* 281:37091–37101.

38. Kooijman, E. E., D. P. Tieleman, …, B. de Kruijff. 2007. An electrostatic/hydrogen bond switch as the basis for the specific interaction of phosphatidic acid with proteins. *J. Biol. Chem.* 282:11356–11364.

39. Yu, A., Y. Xing, …, T. Kirchhausen. 2010. Structural analysis of the interaction between Dishevelled2 and clathrin AP-2 adaptor, a critical step in noncanonical Wnt signaling. *Structure.* 18:1311–1320.

40. Consonni, S. V., M. Gloerich, …, J. L. Bos. 2012. cAMP regulates DEP domain-mediated binding of the guanine nucleotide exchange factor Epac1 to phosphatidic acid at the plasma membrane. *Proc. Natl. Acad. Sci. USA.* 109:3814–3819.

41. Ballon, D. R., P. L. Flanary, …, J. Thorner. 2006. DEP-domain-mediated regulation of GPCR signaling responses. *Cell.* 126:1079–1093.

42. Vance, J. E., and R. Steenbergen. 2005. Metabolism and functions of phosphatidylserine. *Prog. Lipid Res.* 44:207–234.

43. Kooijman, E. E., V. Chupin, …, K. N. Burger. 2003. Modulation of membrane curvature by phosphatidic acid and lysophosphatidic acid. *Traffic.* 4:162–174.

44. van den Brink-van der Laan, E., J. A. Killian, and B. de Kruijff. 2004. Nonbilayer lipids affect peripheral and integral membrane proteins via changes in the lateral pressure profile. *Biochim. Biophys. Acta.* 1666:275–288.

45. Shin, J. J., and C. J. Loewen. 2011. Putting the pH into phosphatidic acid signaling. *BMC Biol.* 9:85.

46. Fang, Y., M. Vilella-Bach, …, J. Chen. 2001. Phosphatidic acid-mediated mitogenic activation of mTOR signaling. *Science.* 294:1942–1945.

47. Veverka, V., T. Crabbe, …, M. D. Carr. 2008. Structural characterization of the interaction of mTOR with phosphatidic acid and a novel class of inhibitor: compelling evidence for a central role of the FRB domain in small molecule-mediated regulation of mTOR. *Oncogene.* 27:585–595.

48. Kooijman, E. E., K. M. Carter, …, B. de Kruijff. 2005. What makes the bioactive lipids phosphatidic acid and lysophosphatidic acid so special? *Biochemistry.* 44:17007–17015.

49. Habas, R., I. B. Dawid, and X. He. 2003. Coactivation of Rac and Rho by Wnt/Frizzled signaling is required for vertebrate gastrulation. *Genes Dev.* 17:295–309.

50. Luo, Z. G., Q. Wang, …, L. Mei. 2002. Regulation of AChR clustering by Dishevelled interacting with MuSK and PAK1. *Neuron.* 35:489–505.

51. Pettersen, E. F., T. D. Goddard, …, T. E. Ferrin. 2004. UCSF CHIMERA—a visualization system for exploratory research and analysis. *J. Comput. Chem.* 25:1605–1612.

52. Cornell, W., P. Cieplak, …, P. A. Kollman. 1995. A second generation force field for the simulation of proteins, nucleic acids, and organic molecules. *J. Am. Chem. Soc.* 117:5179–5197.

53. Cheatham, 3rd, T. E., P. Cieplak, and P. A. Kollman. 1999. A modified version of the Cornell et al. force field with improved sugar pucker phases and helical repeat. *J. Biomol. Struct. Dyn.* 16:845–862.